SCIENCE CHINA
Technological Sciences

•Article•

October 2019 Vol.62 No.10: 1805–1815
https://doi.org/10.1007/s11431-019-9541-3

A new method for deburring of servo valve core edge based on ultraprecision cutting with the designed monocrystalline diamond tool

AN QingLong*, DANG JiaQiang, LIU GongYu, Dong DaPeng, MING WeiWei & CHEN Ming

State Key Laboratory of Mechanical System and Vibration, School of Mechanical Engineering, Shanghai Jiao Tong University, Shanghai 200240, China

Received April 2, 2019; accepted June 12, 2019; published online July 11, 2019

Deburring of high-precision components to their micrometer features without any damage is very important but of great difficulty as the burr-to-functionality size ratio increases. To this end, this paper proposes a new deburring method in which the micro burr should be directly removed based on ultraprecision cutting with the designed monocrystalline diamond tool. To determine the feasibility of the proposed method, this paper applies it for deburring of the precision working edge of the servo valve core. Firstly, the monocrystalline diamond tool is carefully designed by covering a variety of topics like rake angle, clearance angle, edge radius. Then, the finite element (FE) simulation was conducted to characterize the deburring performance during the removal of the micro burr produced by the single abrasive grinding. Finally, an innovative self-designed deburring system was introduced and the deburring process was evaluated in terms of cutting forces, temperatures, tool wear mechanisms and deburring quality of the working edges by experiments. The FE simulation results indicate the suitability of the proposed deburring method. Meanwhile, the experimental findings agree well with simulation results and show that ultraprecision cutting with the specialized monocrystalline diamond tool could be successfully used for deburring of servo valve core edge without any damage. This work can provide technical guidance for similar engineering applications, and thus brings an increase to the machining efficiency for the manufacture of precision components.

monocrystalline diamond tool, FE simulation, deburring method, servo valve core edge, ultraprecision cutting

Citation: An Q L, Dang J Q, Liu G Y, et al. A new method for deburring of servo valve core edge based on ultraprecision cutting with the designed monocrystalline diamond tool. Sci China Tech Sci, 2019, 62: 1805–1815, https://doi.org/10.1007/s11431-019-9541-3

1 Introduction

Traditional cutting processes of metals such as milling, turning, grinding, are extensively applied for manufacturing of the high-precision components with micrometer-sized features in modern industries, due to their accuracy effectiveness and high efficiency [1–4]. Formation of burrs is still one of the biggest challenges faced by the conventional manufacturing operations, which are usually yielded on the workpiece edges owing to lack of support for the flowing material during the cutting/grinding process [5–7]. The burrs should have significant negative impacts on the accuracy and even the functionality of the components. Therefore, the development of deburring processes is of vital importance.

Currently, various deburring methods have been introduced in the literature. According to the principles of the burr removal, these methods can be basically categorized into four types, i.e., the mechanical, electrical, chemical, and thermal deburring operations. As for the mechanical method, it is the typical and traditional method widely used in practical productions. Jang et al. [1] reported a deburring method predominantly depending on the magnetorheological fluid

*Corresponding author (email: qlan@sjtu.edu.cn)

© Science China Press and Springer-Verlag GmbH Germany, part of Springer Nature 2019

with a variable yield stress, which could be controlled by an external magnetic field. The burrs with a height of nearly 200 μm on the micro-molds were removed successfully. Kwon et al. [8] mentioned an abrasive deburring method that utilized a pipe with a hole to move water with an abrasive and a pump for suction. This method could remove the small burrs effectively at the intersecting holes inside the products, but is inapplicable for removal of the large burrs due to the limited deburring force. Damian et al. [9] applied the vibra-abrasive machining for deburring the sharp edges of soft materials, and the experimental results showed that increasing treatment time caused a reduction in the length of burrs. However, in the mechanical method, the problems of over-machining as well as other mechanical damages still need to be carefully avoided with much attention. As for the electrical method, of which the electrical discharge machining (EDM) is the most extensively used. Jeong et al. [10] used the micro EDM with a small-diameter cylindrical tool for deburring the micro-features and achieved promising results only for the conductive materials, such as aluminum, copper, and stainless steels. Islam et al. [11] applied the EDM for removal of burrs during the drilling process of carbon fiber reinforced plastic composites (CFRP). Through the experiments, the copper electrode was tested to perform the best in both of the deburring time and the material removal rate than the steel, brass, and aluminum. However, due to the limitation of electrical discharge conditions, the electrical method can only be used for deburring the conductive materials. As for the chemical method, it is much applicable for removing the burrs inside the deep holes and, among this method, the electrochemical approach is the most widely accepted. Choi and Kim [12,13] developed an electrochemical deburring method by using electroplated cubic boron nitride wheels for the removal of burrs in an internal cross hole and obtained the optimum conditions for the deburring process. On the basis of the burr removal mechanism of electrochemical dissolution, Sarkar et al. [14] developed a mathematical model to evaluate the deburring performances of this method and gave the parametric limits for the proper operation. However, the deburring efficiency of this method still needs to be improved. As for the thermal method, the electron beam (EB) and the laser are the two main sources of energy used for the burr removal purpose. Kim and Park [15] used the large pulsed EB to assist the abrasive deburring for the patterned metal masks, and successfully reduced the size of burrs to approximately 7.2 μm, much less than the results of abrasive deburring alone 38.01 μm. Okada et al. [16] proposed a large-area EB irradiation method with high and uniform energy distribution for instant melting of metal surfaces, thus removing the micro-burrs completely. Experimental results showed that the micro-burrs at the edges of small holes could be removed at once. Besides of the EB, the laser deburring method was also regarded to have an extended degree for the manufacturing automation, but it was found by Möller et al. [17] that the effects of the temperature field on the deburring result were significant, and the burning was easily caused to the material substrate. Moreover, for the thermal method, the low controllability of deburring area is still a big challenge.

Generally, the traditional deburring procedures mentioned above are unsuitable for some acute cases, where the burr-to-functionality size ratio for the precise features at micrometer scale is too high to ignore since it would become of difficulty to remove the burrs effectively without any damage to the micro-features of the workpieces. For instance, the burr height on the precision working edge of servo valve core applied in the rockets and missiles is approximately 5 μm shown in Figure 1 and the burr could not be removed by the above deburring methods since overcut is likely to occur during the deburring process. However, the high-precision manufacturing technologies, such as ultraprecision cutting, are expected to meet these requirements that cannot be achieved by conventional deburring processes and open new technological possibilities for deburring of these precision products due to its high machining accuracy of ultraprecision cutting. For this purpose, this paper proposed a new online deburring method to remove the burrs on the precision working edges of the workpieces based on the ultraprecision cutting (monocrystalline diamond turning), which is particularly suitable for the burrs with micrometer features. This deburring process functions by utilizing a specially designed monocrystalline diamond tool, whose motion precision works in micron scale under the controlling system. In this paper, the performances of the deburring process are quantitatively examined and evaluated through the application for deburring of the working edges of servo valve cores after the

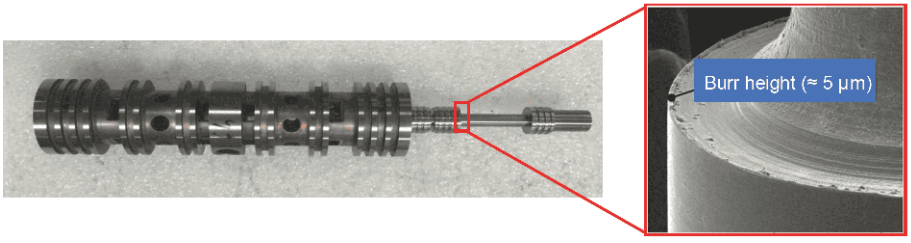

Figure 1 (Color online) Burr appearance and size on the precision working edge of the servo valve core.

end-face grinding operation. A variety of topics, including the cutting forces, temperatures, tool wear and deburring quality of the working edges, are concerned respectively. Besides, the burr removal mechanism is also investigated and explained through the finite element (FE) simulation. The following sections of this paper will describe: (1) the geometrical design of the monocrystalline diamond tool and discussion on the deburring performances based on FE simulation; (2) the experimental setup of the online deburring method/system; (3) the experimental results including the deburring forces, temperatures, tool wear mechanisms, and deburring quality of the working edges.

2 Theoretical investigation

2.1 Geometrical design of the monocrystalline diamond tool

The geometrical parameters of the monocrystalline diamond tool to be designed mainly include the rake angle γ, relief angle α, and the edge radius r. Owing to the significant influence of crystal orientation of the diamond substrate on the cutting performances such as chipping and wear resistance [18], the tool geometry needs to be designed corresponding to the crystal lattice of the monocrystalline diamond. In addition, as for the tool fabrication method of the mechanical lapping, the polishing direction of the lapped tool facet is highly recommended to be parallel to the 'soft' orientation of the diamond. As illustrated by the literatures [18–20], the visible tool wears usually occurred on the flank face of the diamond tool. Therefore, to improve the anti-wear performance of the tool, the flank face should be oriented in order to obtain the high tensile strength in the cutting direction [21]. In this study, the rake face and flank face of the monocrystalline diamond are elaborately designed on the special crystal planes as shown in Figure 2. Specifically, the γ is 6°, α is 10°, the surface roughness Ra is less than 0.01 μm, and the r is 80 nm.

2.2 Evaluation of the deburring performance based on FE simulation

The FE simulation has become an appropriate technique for studying the micro-scale processes in the cutting zone at the millisecond timescale, which cannot be studied experimentally or by analytical calculations [22]. It can model the physical properties of both the tool and the workpiece through meshing the two objects into a large number of discrete nodes. During the simulation, physical variables of the nodes are changed due to the evolution of boundary conditions, which can eventually show the mechanical and thermal variable fields dynamically in the cutting zone as well as the machined surface integrity and tool wear [23]. Owing to the reasonable prediction accuracy for the cutting forces and temperature fields, the FE simulation has been widely accepted and applied in engineering and academia [24–26].

To better understand the mechanism during the removal of micro-burrs and provide theoretical guidance for the feasibility of the proposed method, the FE simulation of the deburring process with a monocrystalline diamond tool is of great significance. To characterize the effectiveness of the deburring simulation, it is necessary to ensure that the burr model in the simulation is in accordance with the actual micro burr. Therefore, the simulation of burr formation in the grinding process with a single abrasive was conducted before the deburring simulation.

2.2.1 Simulation of burr formation

Firstly, the geometry of the single SiC grain was modeled based on the average sizes of the abrasive grains on the grinding wheel used in the production site. The tip radius of the abrasive is 25 μm, and the tip angle is 72°. Secondly, the parameters of the cutting depth and cutting speed of the grain were given based on the actual end-face grinding process. Thirdly, the boundary constraints were given to the workpiece of 440C stainless steel. The process parameters of the simulation for burr formation are: cutting speed is 30 m/s; cutting depth is 6 μm, environment temperature is 20°C, and with no coolant.

In this paper, both the simulation of burr formation and the following deburring process were carried out with the commercial FE simulation software Deform-3D™. The thermal-mechanical behavior of the workpiece in the present work was described by the Johnson-Cook (JC) constitutive model, which depicted the flow behaviors (strain hardening, strain rate sensitivity, and thermal softening) over wide strain and temperature range. The JC model is expressed as follows [27]:

$$\sigma = (A + B\varepsilon^{n})\left(1 + C\ln\frac{\dot{\varepsilon}}{\dot{\varepsilon}_0}\right)\left[1 - \left(\frac{T - T_{\mathrm{r}}}{T_{\mathrm{m}} - T_{\mathrm{r}}}\right)^{m}\right],$$

where σ, ε, $\dot{\varepsilon}$ and T represent the equivalent flow stress, the equivalent plastic strain, the plastic strain rate, and the absolute temperature respectively. The other parameters of the JC model are n (strain hardening exponent), m (thermal softening exponent), A (initial yield stress), B (hardening modulus), C (strain rate sensitivity coefficient), $\dot{\varepsilon}_0$ (reference strain rate), T_{r} (reference temperature) and T_{m} (melting temperature), respectively. The coefficients involved in the JC model used for simulation are listed in Table 1 [28].

The simulation and experimental results of the burr formation were plotted in Figure 3. As can be seen from this figure, when the simulation of the grinding process with a single abrasive was finished, the burr was finally acquired. In comparison to the actual burr obtained through experiments

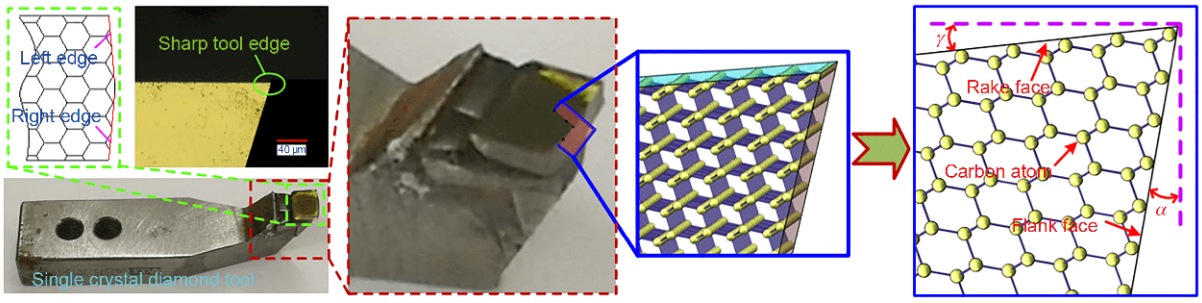

Figure 2 (Color online) Geometrical design of the monocrystalline diamond tool.

Table 1 Coefficients of the JC model for the workpiece material [28]

Coefficient	A (MPa)	B (MPa)	C	M	n	$\dot{\varepsilon}_0$ (s^{-1})	T_m (°C)	T_r (°C)
Value	209.7	1383.2	−0.0095	0.5147	0.915	0.01	1400	20

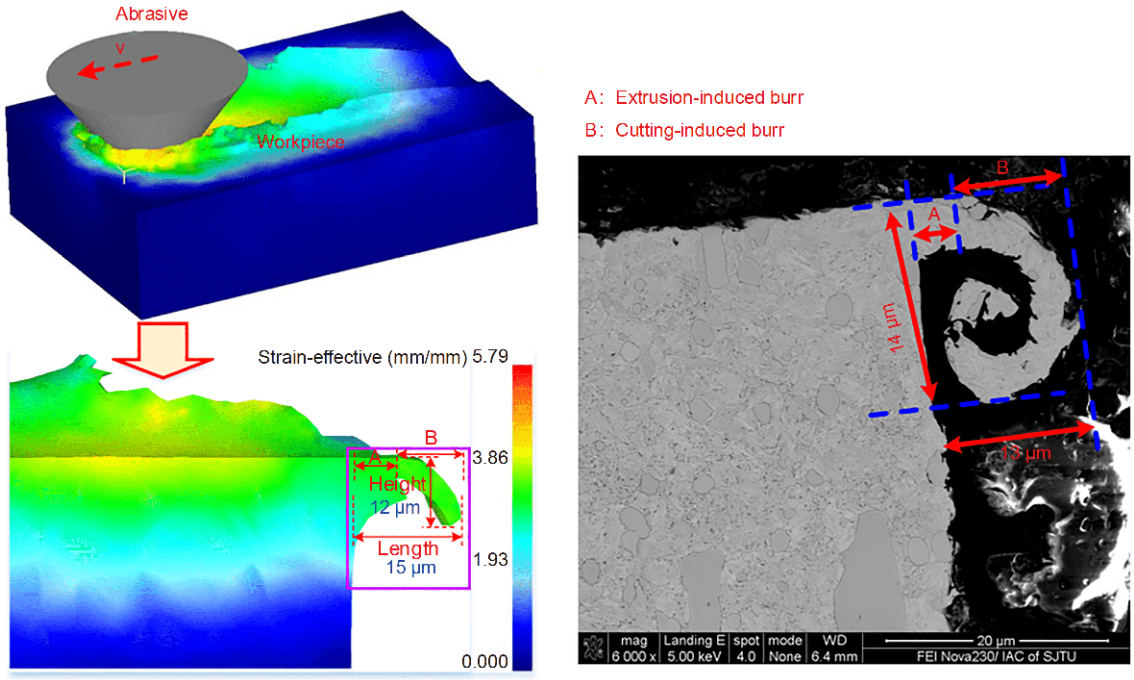

Figure 3 (Color online) The comparison of burr size between simulation and experimental results.

with the same process parameters, it can be noted that the length of the predicted burr is 15 μm, which is 15.4% more than that of the actual burr, and the height of the predicted burr is 12 μm, being 14.3% less than that of the actual burr. Furthermore, the burr morphology obtained by the FE simulation and experiment includes two parts: cutting-induced burr and extrusion-induced burr. The length of cutting-induced burr is slightly shorter in the simulation compared to the experimental results. This phenomenon can be attributed to the premature fracture of the burr in the simulation since the damage parameters adopted in the simulation has inevitable error compared to that in the actual experiments. Whereas the extrusion-induced burr length in the simulation is slightly longer due to that the strain rate hardening of the material under high linear velocity in the experiments is relatively stronger than that described by the FE simulation. In general, it can be concluded that the predicted burr in the simulation agrees well with the actual burr obtained from the experiment. The reasonable simulation of burr formation could contribute to the reliability of the following deburring simulation.

2.2.2 *Simulation of deburring process*

In the deburring simulation, all of the geometrical parameters of the cutting tool, the workpiece, the boundary constraints and process parameters are identical as those used in the

experiments. The room temperature is set as 20°C in the deburring simulation. The cutting speed of the deburring tool was 94 mm/s, which was determined by the linear velocity of the rotating working edge of the servo valve. Upon completeness of simulation, the results could be demonstrated through the postprocessor. In this work, the fundamental physical properties of cutting forces and temperatures in the cutting zone were carefully captured since the cutting force is a most important factor in determining the micro chipping and abrasive wear of tool edges and the temperature is usually the reason of diffusion wear on the tool edges.

Detailed views of the temperature rise field and effective flow stresses field in the cutting region are shown in Figures 4 and 5, respectively. It can be seen from Figure 4 that higher temperature rise existed in the entire burr body than the workpiece substrate, with the highest one on the burr surface that contacted with the tool. The gradient distribution of the temperature rise on the workpiece was obvious, which decreased from the side near the cutting zone to the opposite side due to the heat conduction. As for the effective flow stresses drawn from Figure 5, they only existed in the plastic flowing materials, inducing the cutting force acting on the moving tool. Meanwhile, Figure 5 obviously shows that the effective flow stresses were mainly generated in the burr body, with a concentration at the burr root connecting with the workpiece substrate. Furthermore, the variation of effective flow stress during the deburring process is plotted in Figure 6, in which the flow stress field corresponding to different deburring moments can be characterized clearly.

To determine the evolution of the cutting forces involved in the deburring process, the three-dimensional cutting forces in the deburring simulation were summarized in Figure 7. It is clear that the forces in the three orthogonal coordinates, regardless of the magnitudes, have a similar variation trend. Overall, the whole procedure could be divided into three phases: before deburring, in deburring and after deburring, respectively. The first was an air-cut period. However, the weak fluctuation of cutting forces still occurred in this period due to the friction between the tool flank face and the side face of the workpiece when the tool was moving forward. The second was the cutting period during which the tool contacts directly with the overhanging burr. The cutting force along with the feed direction increased firstly to the maximum of 0.32 N and then decreased with the increment of simulation time. Periodically, the third was also an air-cut period with a small residual force caused by the friction, which was similar to the first period. In particular, the major cutting force F_z was much larger than F_y and F_x, which in-

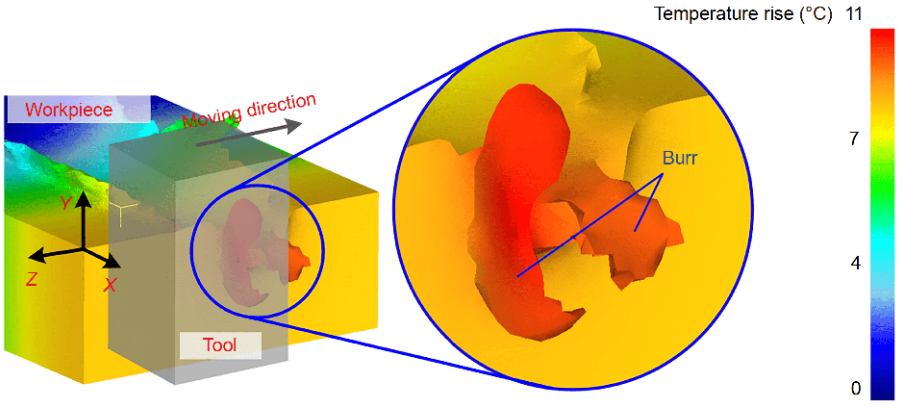

Figure 4 (Color online) Temperature field during the deburring process.

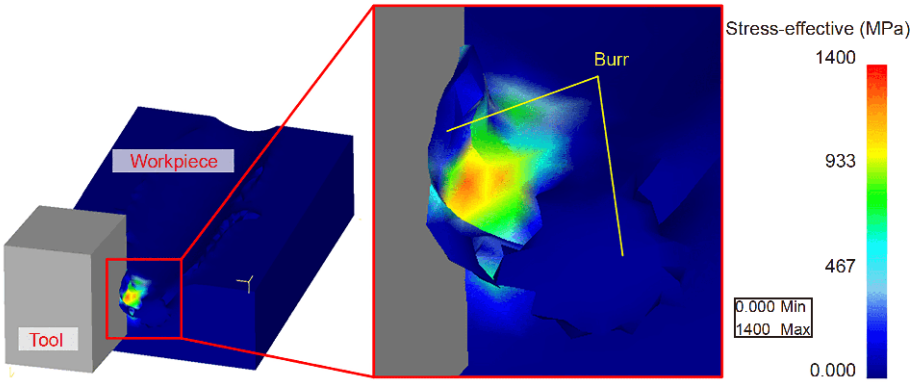

Figure 5 (Color online) Effective flow stresses field during the deburring process.

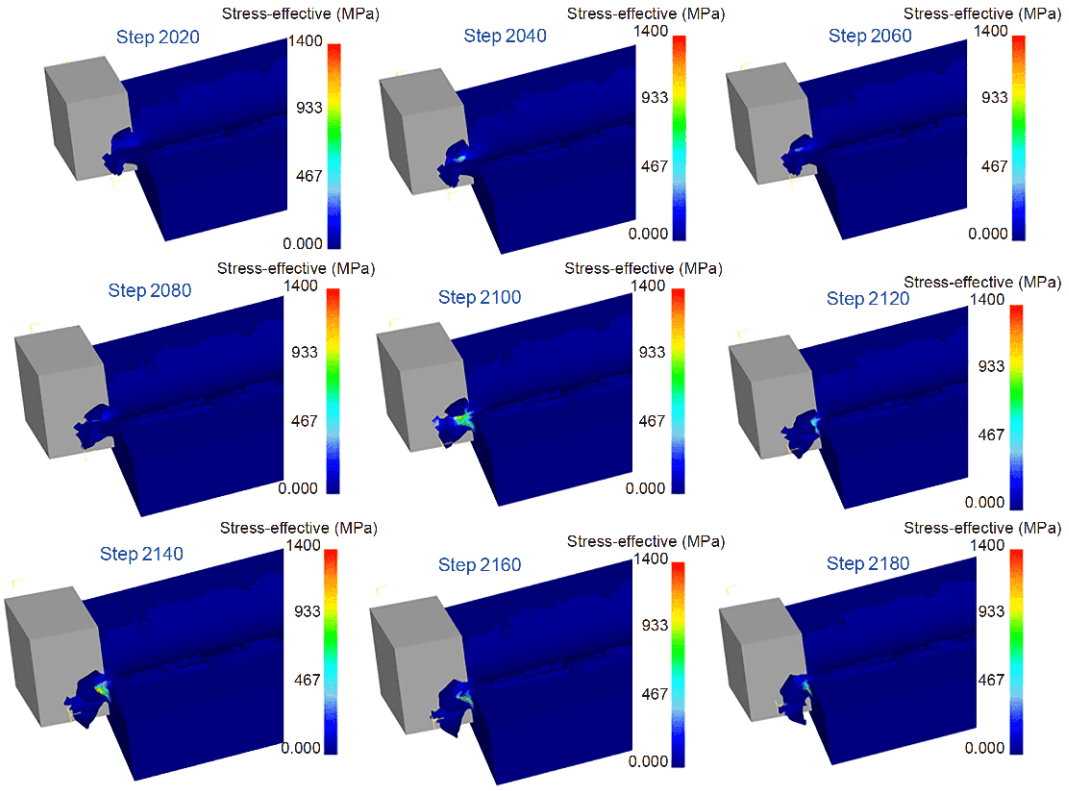

Figure 6 (Color online) The variation of effective flow stress during the deburring process.

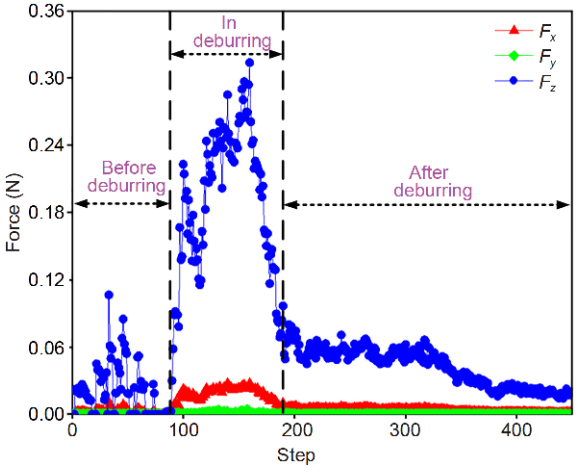

Figure 7 (Color online) Variation of the three-dimensional cutting forces in the deburring simulation.

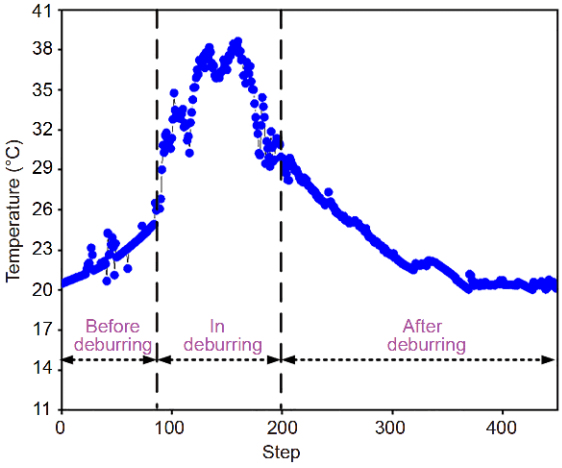

Figure 8 (Color online) Variation of the cutting temperature in the deburring simulation.

dicates the tangential force perpendicular to the burr plays an essential role during the deburring process. Besides, the variation of the cutting temperatures as a function of the simulation step is shown in Figure 8. As can be seen, the temperature exhibited a consistent variation trend with the cutting forces, including three categorical periods as well. This phenomenon indicates that there was a close internal relevance between the two physical quantities. In the first period, the temperature presented a linear growth. In the second period, the temperature increased to a maximum of about 38.1°C and then decreased. In the third period, the temperature showed a linear downward trend with versus simulation step. According to the results, it could be concluded that the temperature was too low to cause chemical reactions to the diamond tool during the deburring process. Indeed, the deburring process is a special case of intermittent

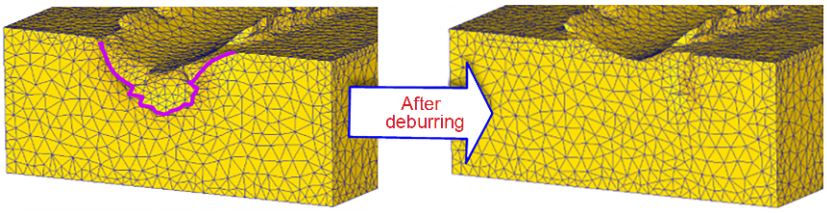

Figure 9 (Color online) Machined surface topographies before and after deburring.

cutting. It can be speculated that the cutting temperature will change in a periodical variation with the alteration of the real-cut and air-cut periods, which will be aggravated in the real-cut periods but moderated in the air-cut periods. Due to this rapid alteration, the duration of the contact between the diamond tool and the workpiece could be limited properly. Therefore, the cutting temperature could be kept below the threshold value, thus the diamond tool wear could be suppressed effectively.

Figure 9 shows the FE simulation results of the 3D morphologies of the machined surface before and after the deburring process. It can be seen that the burr was removed successfully with the monocrystalline diamond tool designed in this paper. This phenomenon also demonstrates the feasibility of cutting with the specialized diamond tool for the removal of micro burrs on the working edges.

3 Experimental validation and discussion

After conducting the simulation of the deburring process, it was shown that the micro burrs can be cut off with the diamond tool. In this section, the experimental validation based on the self-designed online deburring system will be introduced. A variety of deburring experiments for the working edges of servo valve cores were conducted, in which both the cutting forces and temperatures during the deburring process were carefully recorded. Furthermore, the tool wear mechanisms, tool life and the machined surface quality of the working edges of servo valve cores were analyzed.

3.1 Build-up of the experimental equipment

With respect to the manufacturing processes of the servo valve cores, the finish grinding of the end-faces is the last but the most important procedure since it directly determines the machined quality of the components. However, a number of micro burrs are easily to occur on the high-precision working edges along the radial direction of the valve cores when conducting the finish grinding operation of the end-faces. In order to avoid the failure of the functional components, it is urgent to remove the burrs effectively and keep the precise edges intact.

The schematic diagram of the online deburring system with a monocrystalline diamond tool for deburring of the precise working edge of a servo valve core is illustrated in Figure 10. In this investigation, the length of the burrs on the working edges used for the experiment was about 14 μm measured by the contour graph software (Think Focus SM-1000 3D) as shown in Figure 11. Therefore, the effectiveness and reliability of the deburring process depended not only on the cutting tool but also on the positioning accuracy of the involved equipment. Due to the high positioning accuracy of 0.1 μm of the deburring system designed in this paper, the burrs should be removed precisely by ultraprecision cutting with the monocrystalline diamond tool. The cantilever force sensor (FUTEK LBB200) with a measuring accuracy of 0.005 N and measuring range of ±4.5 N can be fully qualified for measuring the deburring force accurately. The on-site experimental setup of the automatic online deburring system for the precision working edges of the servo valve cores during the end-face grinding process is shown in Figure 12.

It should be noted that the ultraprecision cutting used for deburring proposed in this paper is similar to the diamond turning process. When conducting the deburring process, the diamond tool will be moved to contact with the workpiece edge where burrs exist. During the rotation of the workpiece, the burrs on the working edges could be directly cut off by the designed diamond tool, thus realizing the successful removal of the burrs. This method could assure the availability of the deburring process, especially for the micro burrs.

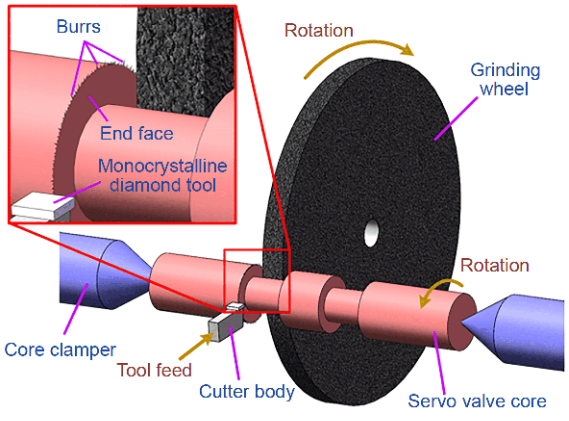

Figure 10 (Color online) Schematic diagram of the online deburring process with a monocrystalline diamond tool.

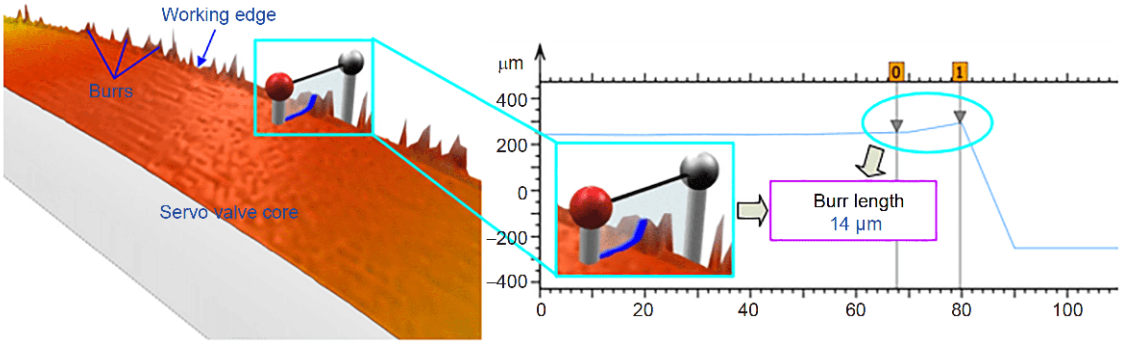

Figure 11 (Color online) Characterization of the burr sizes existed on the working edge of the servo valve core.

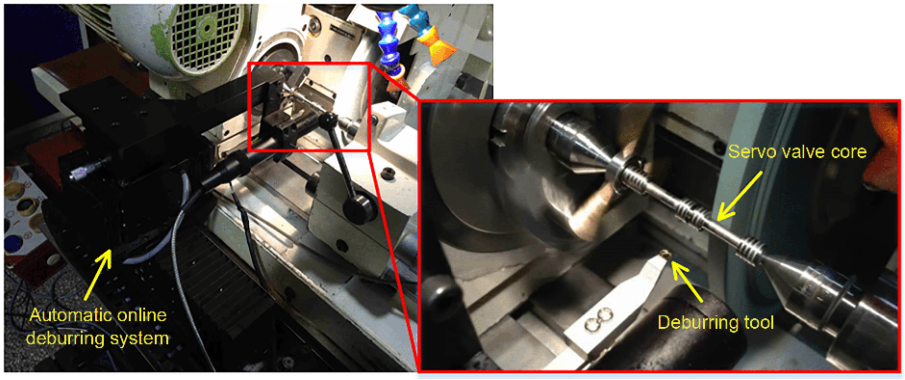

Figure 12 (Color online) The high-precision automatic online deburring equipment.

3.2 Results of cutting forces and temperatures

Based on the specialized monocrystalline diamond tool and the established deburring system, a series of deburring trials were carried out. It should be noted that the deburring experiments were conducted in the room that has a constant temperature of 20°C, which is the same as the simulated condition. During the deburring process, the cutting force was measured by the cantilever force sensor attached to the tool. Besides, the deburring temperature was measured by a high-precision infrared thermograph (FLIR A65). Due to the extremely short duration of the engagement between the tool and the burrs, the maximum force, as well as the maximum temperature in the period of deburring, were recorded out of an entire working edge for evaluating the deburring performance. In this way, the recorded maximum cutting forces in deburring 10 working edges were shown in Figure 13, in comparison with the predicted ones obtained through the FE simulation. It can be seen that the average value of the experimental cutting forces is 0.47 N, while the maximum predicted force is 0.32 N, being about 32% lower than the experimental one. The reason accounting for this distinction between the simulation and experiment result could be that the forces measured in experiments may contain not only the deburring force but also the additional force caused by the extrusion and friction of the tool flank face with the machined surface of the workpiece. Moreover, the boundary condition set in the FE simulation was likely to be incompletely identical with the actual experimental situations. In Figure 14, the average value of the measured cutting temperatures recorded in experiments is 34.5°C, while the maximum predicted cutting temperature is 38.1°C being just about 10% higher than the experimental one. Considerably, the experimental results have confirmed the reasonability of the simulation results.

3.3 Tool life and tool wear mechanisms

Through a series of deburring experiments, the tool life of the designed monocrystalline diamond tool was tested. It was found that the tool could cut off the burrs effectively with a cumulative number of approximately 400 working edges of servo valve cores, until any overcut, undercut, or even scrapping occurred. After the experiments, the tool was cleaned by acetone and the wear features were taken to be observed by the optical microscope (Keyence VHX-600). The OM photographs of the tool rake face before and after deburring 100 working edges are shown in Figure 15(a) and (b), respectively.

Apparently, few damages appeared on both the tool cutting edge and rake face after the deburring process of 100

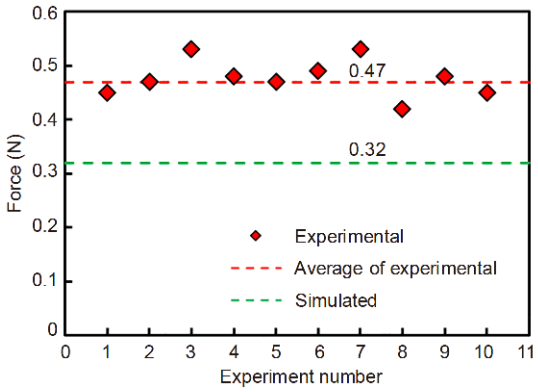

Figure 13 (Color online) Comparison of cutting forces between experiments and simulation.

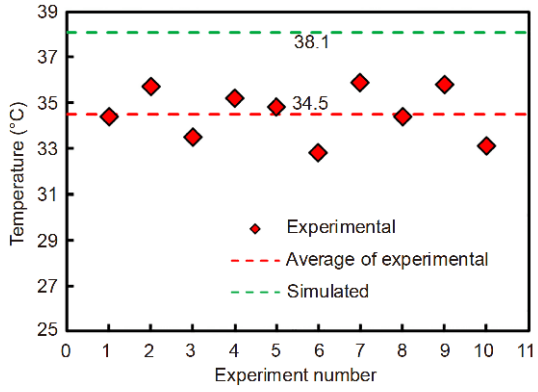

Figure 14 (Color online) Comparison of cutting temperature between experiments and simulation.

working edges. Furthermore, Figure 16 demonstrates the enlarged views of the rake face and the flank face of the diamond tool after the deburring of 400 working edges, respectively. On one hand, it can be seen that there were only a few small diffusion spots induced by the excessive cutting temperature in both the rake face and the flank face, indicating that the temperatures during the deburring process were relatively low. On the other hand, it is clear that the main wear mechanism of the tool was micro-chipping. Besides, no significant signs of the mechanical abrasion due to the friction between the tool and workpiece existed on the diamond tool. This phenomenon could be attributed to the favorable wear-resistance of the diamond material. Suffering the repeated impact of the deburring forces, the sharp tool edge used in the deburring system was prone to micro-chipping. In addition, more diffusion spots were generated on the tool rake face than that on the flank face. This behavior can be attributed to the fact that the temperature in the rake face was higher than that in the flank face during the deburring process. Much more heat was generated in the primary deformation zone of the burr near the rake face due to the shear stress in the workpiece material, than that in the second deformation zone near the flank face due to the friction between the tool flank face and the machined surface of the workpiece.

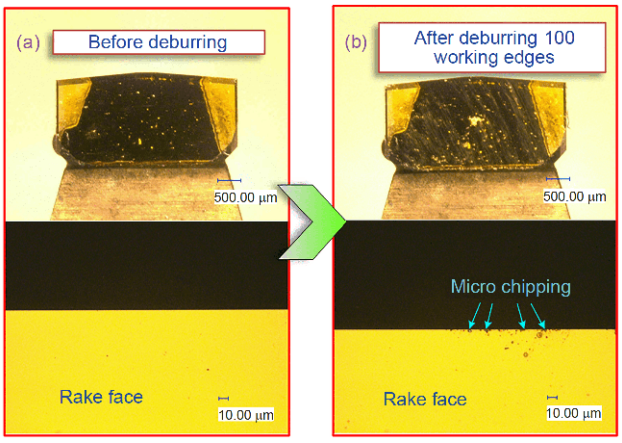

Figure 15 (Color online) Microphotographs of the tool rake face (a) before and (b) after deburring 100 working edges.

3.4 Deburring quality of working edges

The working edges of servo valve cores selected from the experiments between before and after the deburring process are shown in Figure 17. Note that the micro burrs are successfully removed and the qualified edges are obtained by

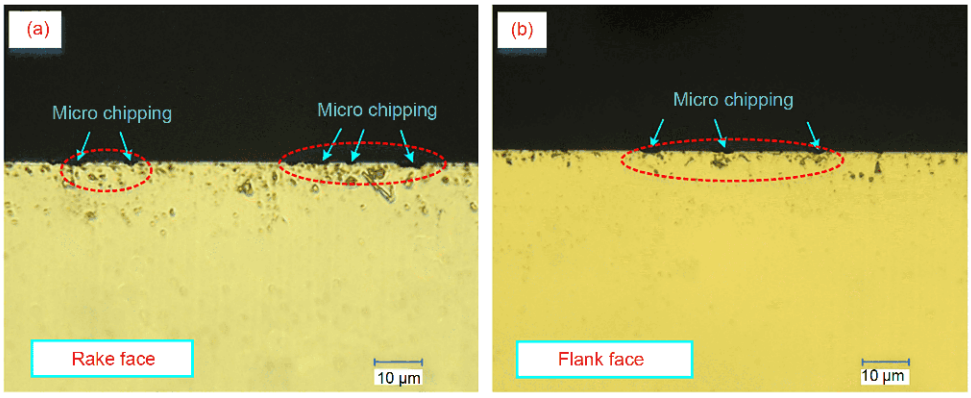

Figure 16 (Color online) Microphotographs of tool face after deburring tests. (a) Rake face; (b) flank face.

ultraprecision cutting with the designed monocrystalline diamond tool. Meanwhile, a typical working edge of the servo valve core randomly selected from the deburred ones was characterized by the 3D profile software as shown in Figure 18. It is clear that there were no overcut or any micro burrs left on the edge, which could meet the machining requirements. The designed monocrystalline diamond tool successfully utilized for deburring of about 400 working edges tested in this study was applicable for the practical deburring procedure of servo valve cores in factories, which could definitely decrease the cost of the deburring process. Furthermore, the efficiency of the deburring method pro-

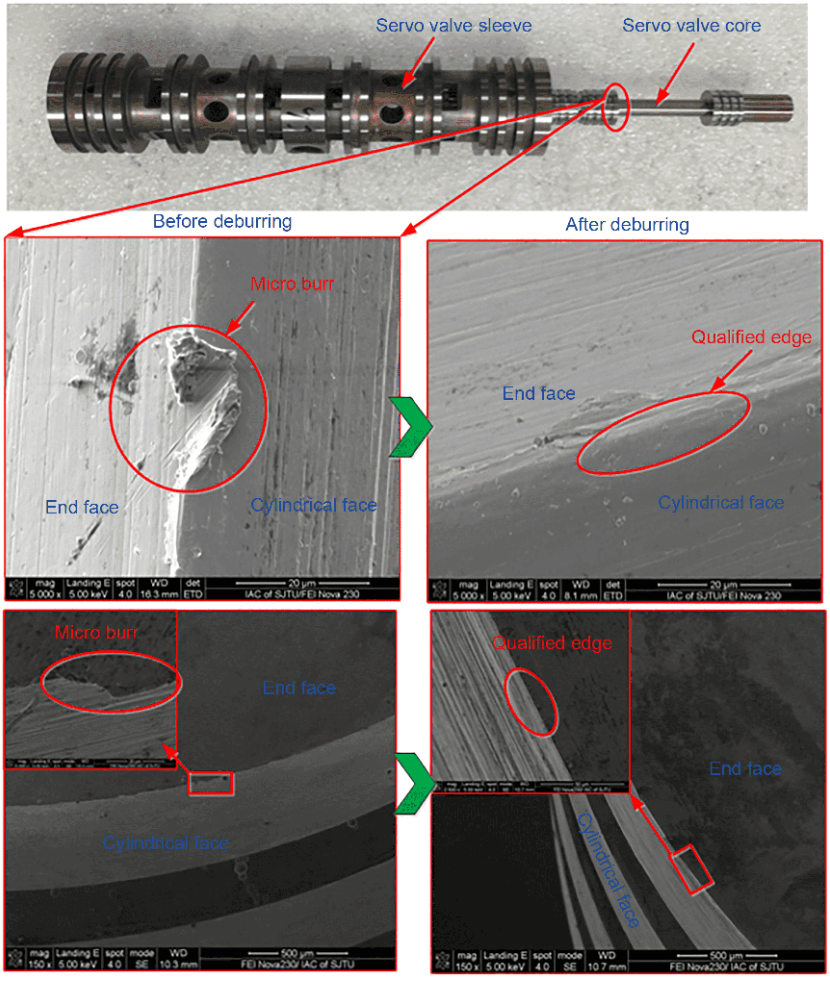

Figure 17 (Color online) Comparison of working edges between before and after the deburring process.

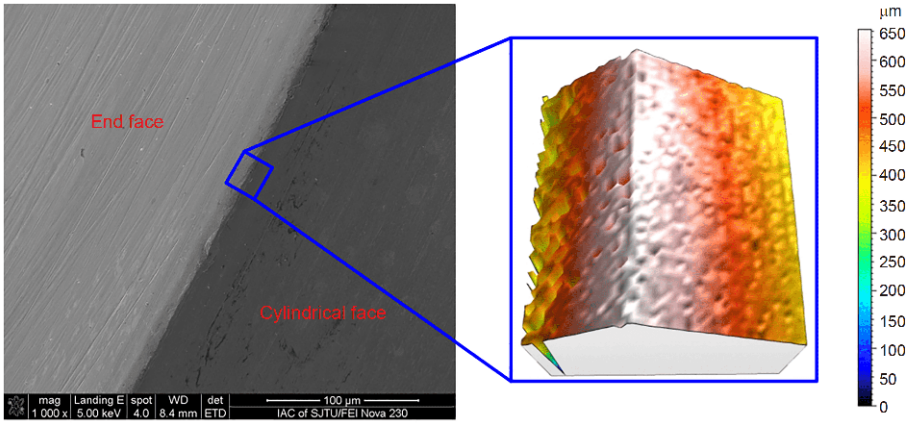

Figure 18 (Color online) Confocal image showing the morphology of the servo valve core after deburring.

posed in this study is proved to be 70% higher than that of the traditional manual deburring method in factories, showing a promising application for practical productions.

4 Conclusions

This paper presents a new deburring approach for removing the micro burrs based on the ultraprecision cutting with the specialized monocrystalline diamond tool. Both the FE simulations and experimental validations were carried out to investigate the feasibility of the proposed deburring method. Through the application for deburring the precise working edges of servo valve cores after the end-face grinding operation, the performances of the deburring process were quantitatively examined and evaluated. Based on the obtained results, some significant conclusions are drawn as follows.

(1) The FE simulation results explained that the alteration of the real-cut and air-cut periods of the diamond tool kept the cutting temperature under the threshold value and contributed to the suppression of tool wear.

(2) Experimental results gained in deburring of the working edges of servo valve cores after the end-face grinding process showed that the deburring force was about 0.47 N, the temperature was about 34.5°C, the primary mechanism of tool wear was micro-chipping, and the designed monocrystalline tool could be used for deburring of approximate 400 working edges of servo valve cores successfully.

(3) The experimental findings coincide well with the simulation result in terms of the cutting forces and temperatures. Both the simulation and experimental results illustrate the feasibility of ultraprecision cutting with the designed monocrystalline diamond tool used for deburring of servo valve core edges.

Besides, it should be noted that the deburring method along with the online deburring system based on the specialized monocrystalline diamond tool proposed in this paper could improve the deburring efficiency greatly, and bring an increase to the machining quality of precise components.

This work was supported by the National Key R&D Program of China (Grant No. 2018YFB2002200).

1 Jang K I, Kim D Y, Maeng S, et al. Deburring microparts using a magnetorheological fluid. Int J Mach Tool Manu, 2012, 53: 170–175
2 Chen J Y, Jin T Y, Tian Y J. Development of an ultrahard nanotwinned CBN micro tool for cutting hardened steel. Sci China Tech Sci, 2016, 59: 876–881
3 Yuan H, Wan M, Yang Y. Design of a tunable mass damper for mitigating vibrations in milling of cylindrical parts. Chinese J Aeronaut, 2019, 32: 748–758
4 Wan M, Gao T Q, Feng J, et al. On improving chatter stability of thin-wall milling by prestressing. J Mater Process Technol, 2019, 264: 32–44
5 Han X S, Hu Y Z. Analysis micro-mechanism of burrs formation in the case of nanometric cutting process using numerical simulation method. Sci China Ser E-Tech Sci, 2007, 50: 129–137
6 Wang G C. Transformation of feed-direction burr morphology in turning. Chin Sci Bull, 1996, 41: 520
7 Aurich J C, Dornfeld D, Arrazola P J, et al. Burrs—Analysis, control and removal. CIRP Ann, 2009, 58: 519–542
8 Kwon B C, Kim K H, Kim K H, et al. New abrasive deburring method using suction for micro burrs at intersecting holes. CIRP Ann, 2016, 65: 145–148
9 Damian B, Daniel K, Piotr M. Deburring and smoothing the edges using vibro-abrasive machining. Procedia Eng, 2017, 192: 28–33
10 Jeong Y H, HanYoo B, Lee H U, et al. Deburring microfeatures using micro-EDM. J Mater Process Technol, 2009, 209: 5399–5406
11 Islam M M, Li C P, Won S J, et al. A deburring strategy in drilled hole of CFRP composites using EDM process. J Alloys Compd, 2017, 703: 477–485
12 Choi I H, Kim J D. Electrochemical deburring system using electroplated CBN wheels. Int J Mach Tool Manu, 1998, 38: 29–40
13 Choi I H, Kim J D. A study of the characteristics of the electrochemical deburring of a governor-shaft cross hole. J Mater Process Technol, 1998, 75: 198–203
14 Sarkar S, Mitra S, Bhattacharyya B. Mathematical modeling for controlled electrochemical deburring (ECD). J Mater Process Technol, 2004, 147: 241–246
15 Kim J, Park H W. Hybrid deburring process assisted by a large pulsed electron beam (LPEB) for laser-fabricated patterned metal masks. Appl Surf Sci, 2015, 357: 1676–1683
16 Okada A, Yonehara H, Okamoto Y. Fundamental study on microdeburring by large-area EB irradiation. Procedia CIRP, 2013, 5: 19–24
17 Möller M, Conrad C, Haimerl W, et al. IR-thermography for quality prediction in selective laser deburring. Phys Procedia, 2016, 83: 1261–1270
18 Choi I H, Kim J D. Development of monitoring system on the diamond tool wear. Int J Mach Tool Manu, 1999, 39: 505–515
19 Zong W J, Li D, Sun T, et al. Contact accuracy and orientations affecting the lapped tool sharpness of diamond cutting tools by mechanical lapping. Diamond Relat Mater, 2006, 15: 1424–1433
20 Zong W J, Sun T, Li D, et al. Design criterion for crystal orientation of diamond cutting tool. Diamond Relat Mater, 2009, 18: 642–650
21 Goel S, Luo X, Reuben R L, et al. Influence of temperature and crystal orientation on tool wear during single point diamond turning of silicon. Wear, 2012, 284-285: 65–72
22 Jafarian F, Imaz Ciaran M, Umbrello D, et al. Finite element simulation of machining Inconel 718 alloy including microstructure changes. Int J Mech Sci, 2014, 88: 110–121
23 Rotella G, Dillon Jr. O W, Umbrello D, et al. Finite element modeling of microstructural changes in turning of AA7075-T651 alloy. J Manuf Process, 2013, 15: 87–95
24 Arrazola P J, Özel T, Umbrello D, et al. Recent advances in modelling of metal machining processes. CIRP Ann, 2013, 62: 695–718
25 Umbrello D, M'Saoubi R, Outeiro J C. The influence of Johnson-Cook material constants on finite element simulation of machining of AISI 316L steel. Int J Mach Tool Manu, 2007, 47: 462–470
26 Lu J, Chen J, Fang Q, et al. Theoretical analysis and finite element simulation of Poisson burr in cutting ductile metals. Simul Model Pract Th, 2016, 66: 260–272
27 Johnson G R, Cook W H. A constitutive model and data for metals subjected to large strains, high strain rates and high temperatures. In: The Seventh International Symposium on Ballistics. The Hague, 1983. 541–547
28 Gupta A K, Krishnamurthy H N, Singh Y, et al. Development of constitutive models for dynamic strain aging regime in Austenitic stainless steel 304. Mater Des, 2013, 45: 616–627